Mechanistic Differences between Electrochemical and Gas-Phase Thermal Oxidation of Platinum-Group Transition Metals As Discerned by Surface-Enhanced Raman Spectroscopy

Ho Yeung H. Chan,[†] Shouzhong Zou,[‡] and Michael J. Weaver*,[†]

School of Chemical Engineering and Department of Chemistry, Purdue University, West Lafayette, Indiana 47907

Received: July 21, 1999

The oxidation of five Pt-group metals—platinum, palladium, iridium, rhodium, and ruthenium—is examined by means of surface-enhanced Raman spectroscopy (SERS) in aqueous electrochemical and gaseous dioxygen environments as a function of electrode potential and temperature, respectively, with the objective of intercomparing systematically the conditions required for surface oxide formation and discerning the reaction mechanisms involved. The SERS strategy, utilizing ultrathin Pt-group metal films electrodeposited on a gold substrate, enables monolayer-level metal oxide vibrational spectra to readily be obtained in both the electrochemical and gaseous environments. The SER spectra obtained during positive- and then negative-going potential excursions in aqueous 0.1 M $HClO_4$ display metal−oxygen vibrational bands signaling anodic oxide formation and subsequent removal at potentials consistent with corresponding voltammetric data. The nature of the amorphous oxides (or hydroxides) formed is deduced by comparison with bulk-phase metal oxide Raman spectra. The onset potentials for surface oxide formation are comparable to the thermodynamic potentials for the bulk-phase metal oxides. In contrast, the onset of surface oxidation even in ambient-pressure dioxygen uniformly requires elevated temperatures, ≥200 °C for each metal except for iridium, where oxide formation occurs at ca. 100 °C. While spectral differences are evident, especially on palladium and ruthenium, the nature of the oxides formed in the electrochemical and gaseous systems is largely similar. The highly activated nature of the gaseous O_2 oxidations is consistent with literature reports for Pt-group surfaces in ultrahigh vacuum as well as higher-pressure conditions. Likely reasons for the markedly more efficacious metal electrooxidations are discussed. Thermodynamic factors are not responsible, since the free-energy driving forces for the gaseous O_2 oxidations are larger than for the electrochemical reactions at the applied potentials where surface oxidation for the latter processes proceeds at room temperature. The electrostatic driving forces for oxygen incorporation into the metal lattice (via "high-field ion transport") are also typically more favorable for the gaseous systems, as evidenced by a comparison of the metal−solution and metal−gas surface potentials. The *intrinsically* more facile electrochemical processes thereby deduced are attributed to the occurrence of direct oxide production via a metal−oxygen place-exchange mechanism, expedited by interfacial solvation and therefore being energetically unfavorable in the anhydrous gas-phase environment. Other factors, such as the formation of precursor chemisorbed oxygen, are also considered.

Introduction

Understanding the factors controlling the nature and occurrence of surface oxidation of metals in ambient environments constitutes an issue having enormous technological as well as fundamental importance. Broadly speaking, the bulk of the experimental insight has been attained by means of two markedly disconnected approaches, referring to very different reaction environments. The first involves electrochemical oxidation in aqueous solution. These processes have been scrutinized primarily by conventional electrochemical methods, i.e., faradaic current−potential−time measurements, especially by cyclic voltammetry.[1] While the aqueous electrochemical environment provides a unique means of controlling as well as examining the thermodynamics and kinetics of surface oxidation, information on the oxide structure is largely lacking. The second, quite disparate, type of oxidizing reaction environment examined extensively involves clean metal surfaces dosed with dioxygen in ultrahigh vacuum (UHV).[2] As is well-known, the use of UHV conditions provides a unique degree of control on the surface composition and enables a plethora of microscopic-level surface characterization techniques to be utilized. A key limitation, especially for noble metals, however, is that the extent of surface oxidation under UHV conditions is often very different from that occurring under the ambient pressure oxidizing conditions having more practical relevance, i.e., the so-called "pressure-gap" restriction applies.

This laboratory has been interested for some time in harnessing surface-enhanced Raman scattering (SERS) as a means of examining interfacial oxidations, along with a variety of other adsorption and reactive processes, on noble-metal substrates in electrochemical[3] and gaseous systems.[4,5] The key virtue of SERS is that it provides a vibrational spectral assay with unique sensitivity and surface selectivity over wide frequency ranges, including the low wavenumbers (ca. 200−900 cm^{-1}) where metal−oxygen vibrations are commonly located and is readily applicable to metal−solution, metal−gas, and related ambient

* Corresponding author. Tel: (765) 494-5466. Fax: (765) 494-0239. E-mail: mweaver@purdue.edu.
† School of Chemical Engineering.
‡ Department of Chemistry.

10.1021/jp992500o CCC: $18.00
Published on Web 11/25/1999

interfaces. An apparent limitation is that the SERS effect itself is attainable, at least in optimal fashion with visible laser excitation, on only a few substrates, namely silver, copper, and gold.[6] However, we have shown that the effect can readily be extended to a variety of other surface materials, most prominently Pt-group transition metals, by electrodeposition as ultrathin films on gold.[4] Recent modifications in the electrodeposition procedures, moreover, provide essentially "pinhole-free" films, displaying both near-optimal SERS activity yet free from spectral and chemical interference from the underlying gold substrate.[7,8]

We have utilized this SERS strategy in a number of separate studies of surface oxide formation on noble metals in both aqueous electrochemical[3,4] and gaseous environments,[5] the latter involving primarily dioxygen and nitric oxide at elevated temperatures. The surface oxidation of Pt-group metals is of central relevance to their catalytic properties in both electrochemical and gaseous chemical systems. The individual foci of these studies, however, have been quite diverse. For example, combined SERS and ex situ X-ray photoelectron spectroscopy (XPS) studies have been undertaken to elucidate rhodium[5b] and ruthenium oxide[5e] stoichiometries formed from gaseous dioxygen at elevated temperatures, and the reactivity of rhodium and palladium oxides toward gaseous reductants has been examined by means of transient SERS measurements.[5f−h] Electrochemical SERS measurements have been concerned, for example, with correlating cyclic voltammetric and surface vibrational responses[3b] and the relations between the oxidation of carbon monoxide and surface oxide formation.[4]

The availability of this common vibrational spectral probe in such physically disparate environments offers intriguing opportunities for intercomparing both the nature of the processes involved and the surface oxides thus formed. The objective of the present article is to provide a comparative examination of the initial stages of oxidation of five Pt-group surfaces—platinum, palladium, iridium, rhodium, and ruthenium—in electrochemical and gaseous environments, specifically aqueous acidic solution and dry ambient-pressure dioxygen, by means of SERS. While measurements of this type have been described for some individual systems in earlier reports from this laboratory, the opportunity is taken here to undertake a systematic interrelated survey. A detailed assessment is also provided herein of the extant literature on surface oxidation of these metals in relation to our SERS findings. Intriguingly, the occurrence of transition-metal surface oxidation, readily attainable in aqueous solution at room temperature, is generally found to require elevated temperatures (chiefly ≥200 °C) in the presence of even ambient-pressure dry dioxygen. The kinetic factors limiting the occurrence of such gas-phase surface oxidation with O_2 and other oxidants (e.g., nitrogen dioxide) are considered, along with the likely reasons for the markedly more efficacious surface oxidation occurring in aqueous electrochemical environments.

Experimental Section

Most details of the electrochemical and gas-phase SERS measurements can be found in refs 9 and 10, respectively. A Spectra Physics Stabilite (Model 2017) Kr^+ laser provided the Raman excitation at 647.1 nm with ca. 30 mW incident power on the surface. Scattered light was collected into a SPEX Triplemate spectrometer equipped with a Photometrics CCD detector. The gold templates were either a 0.4 cm diameter rod sheathed in Teflon (for electrochemical experiments) or a 0.6 cm diameter gold foil (99.95%, Alfa-Aesar) mounted on a holder

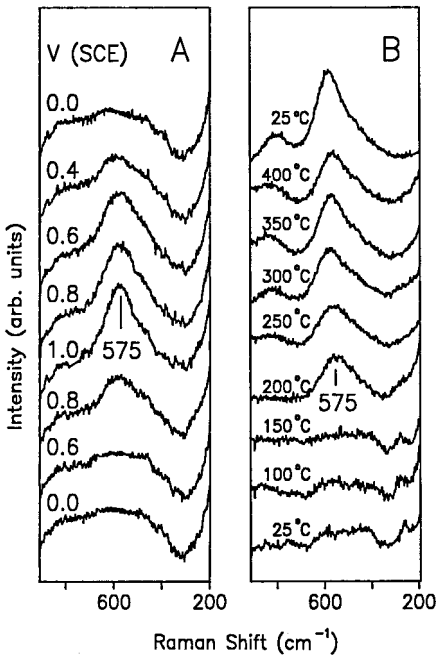

Figure 1. (A) Potential-dependent surface-enhanced Raman (SER) spectra acquired for electrochemical oxidation and subsequent reduction of a platinum film in 0.1 M $HClO_4$. The initial potential was 0 V vs SCE (bottom spectrum), followed by potential increments of 0.2 V up to 1.0 V and finally returning to 0 V. (B) Temperature-dependent SER spectra acquired for thermal oxidation of a platinum film in 1 atm of flowing O_2. The initial reduced surface was obtained by prior thermal treatment in flowing H_2 at 150 °C (bottom spectrum). The temperature was increased typically in 50 °C increments before decreasing back to 25 °C. All the spectra were acquired at the indicated temperatures after the surface reached thermal equilibrium for ca. 2 min.

(for variable-temperature gas-phase experiments). The gold surface was roughened to create optimal (and stable) SERS activity by means of 25 oxidation−reduction cycles in 0.1 M KCl, entailing 1 V s^{-1} sweeps from −0.3 to +1.2 V vs saturated calomel electrode (SCE) and return, holding at the negative limit for 30 s each time.[11] The iridium and ruthenium films were deposited as described in refs 7b and 4b, respectively, while the other three metals deposited as outlined in ref 7a. Conditions were arranged so as to produce transition-metal thicknesses of ca. 3−5 monolayers, thereby yielding near-optimal SERS properties.[7a] In situ electrochemical SERS experiments were performed in a conventional three-electrode cell with a quartz optical window. All potentials were measured and are quoted versus the SCE.

Results and Discussion

Overall Strategies. The experiments described here all involve examining in comparative fashion the initial occurrence of surface oxidation as sensed by SERS for five metals—platinum, palladium, iridium, rhodium, and ruthenium—induced either by altering the metal electrode potential to progressively higher values in aqueous solution, specifically 0.1 M $HClO_4$, or by progressive heating in an ambient pressure of dry flowing oxygen. While several of these systems have been described separately in previous reports from this laboratory, for either the electrochemical or gaseous oxidation modes (see specific references cited below), it is nonetheless instructive to present representative potential- and temperature-dependent SER spectra systematically for each surface. To this end, displayed in Figures 1−5 are SER spectra in the 200−900 cm^{-1} region, where the

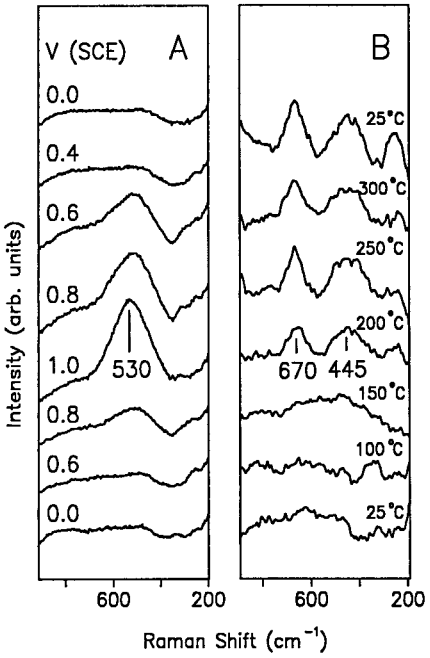

Figure 2. (A) Potential-dependent SER spectra acquired for electrochemical oxidation and subsequent reduction of palladium in 0.1 M $HClO_4$, obtained similarly to Figure 1A. (B) Temperature-dependent SER spectra acquired for thermal oxidation of palladium in 1 atm of flowing O_2, similarly to Figure 1B.

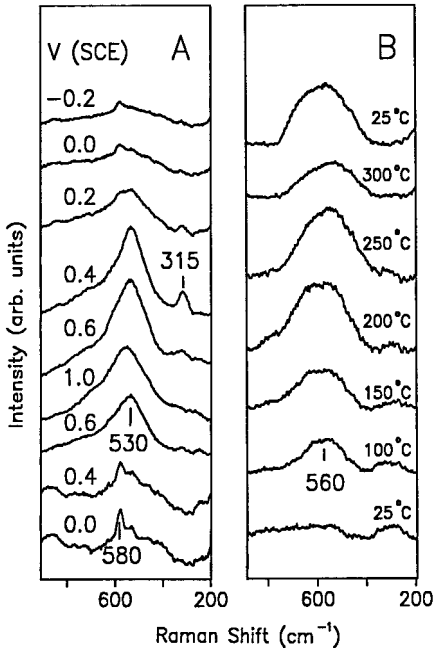

Figure 3. (A) Potential-dependent SER spectra acquired for electrochemical oxidation and subsequent reduction of iridium in 0.1 M $HClO_4$, similarly to Figure 1A. (See text for surface pretreatment details.) (B) Temperature-dependent SER spectra acquired for thermal oxidation of iridium in 1 atm of flowing O_2, similarly to Figure 1B. The reduced surface (bottom spectrum) was obtained by exposure to CO-saturated 0.1 M $HClO_4$ at −0.3 V, sample transfer through air with the CO protective adlayer to avoid atmospheric oxidation, followed by thermal desorption of CO at 200 °C (see text).

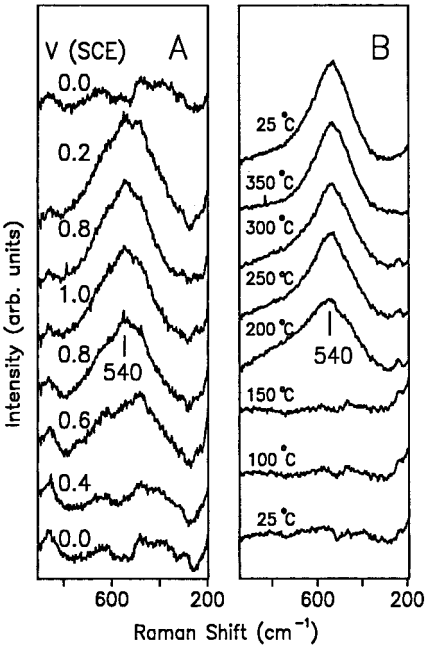

Figure 4. (A) Potential-dependent SER spectra acquired for electrochemical oxidation and subsequent reduction of rhodium in 0.1 M $HClO_4$, similarly to Figure 1A. (B) Temperature-dependent SER spectra acquired for thermal oxidation of rhodium in 1 atm of flowing O_2, similarly to Figure 1B.

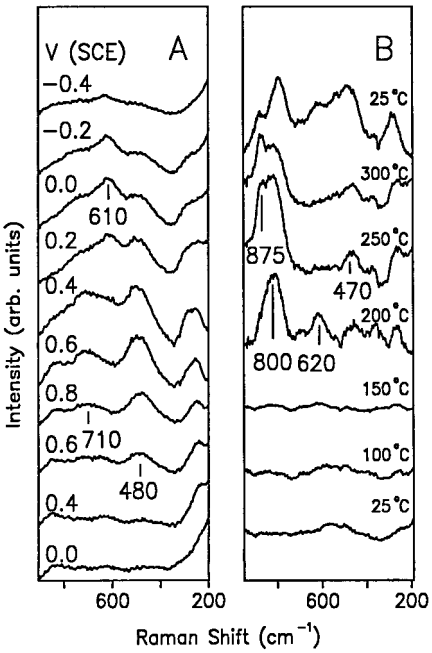

Figure 5. (A) Potential-dependent SER spectra acquired for electrochemical oxidation and subsequent reduction of ruthenium in 0.1 M $HClO_4$, similarly to Figure 1A. (B) Temperature-dependent SER spectra acquired for thermal oxidation of ruthenium in 1 atm of flowing O_2, similarly to Figure 1B. The surface was protected during transfer through air by chemisorbed CO, similarly to iridium (Figure 3B).

metal−oxygen vibrational bands are located. The left- and right-hand sequences (labeled A and B, respectively) refer to electrode potential-dependent spectra obtained in aqueous 0.1 M $HClO_4$ and temperature-dependent spectra acquired in 1 atm. O_2.

The initial electrode potentials in Figures 1A−5A were chosen to be sufficiently low so as to provide a reduced metal surface, as also seen from the largely featureless SER spectra. The potential was then increased in 0.2 V increments to a value (typically 0.8−1.0 V vs SCE) where the initial stage of oxidation is complete, as gleaned partly from the vibrational spectra, stacked upward with time. Approximately 20 s was spent at each potential, forming a staircase potential−time sequence. The

TABLE 1: Raman Vibrational Frequencies (cm^{-1}) for Surface Oxides Formed in Electrochemical and Gaseous Environments and Comparisons with Bulk-Phase Spectra and Frequencies for Adsorbed Atomic Oxygen

		metal oxide raman spectra		
		SERS[b]		
metal	adsorbed atomic oxygen EELS[a]	electrochemical	gas phase	bulk metal oxide[c]
Pt	470 (111)[12]	575	575	440, 660 (PtO)[18] 510, 550 (PtO_2)[18] 570 (amorphous Pt oxide)[18]
Pd	480 (111)[13]	530	445, 670	445, 650 (PdO)[19]
Ir	550 (111)[14]	530	550	550 (IrO_2)[20]
Rh	520 (111)[15] 410 (100)[16]	540	540	530[5b] (amorphous Rh_2O_3) 425, 570, 615[5b,18] (Rh_2O_3)
Ru	500−600 (001)[17]	480, 610, 710	470, 620 800, 875	530, 645[21] (RuO_2) 880 (RuO_4)[22]

[a] Frequencies of metal surface−oxygen stretching vibration for atomic oxygen adlayers on low-index surfaces, as indicated, from electron energy loss spectroscopy, taken from references cited. The range of values given for Ru(001) reflects marked coverage dependence.[17] [b] Frequencies of surface oxide vibrations in either electrochemical or gas-phase environments, taken from SER spectra in Figures 1A−5A and Figures 1B−5B, respectively. [c] Frequencies of major Raman vibrational bands for bulk-phase metal oxides, taken from references cited.

surface oxide can be removed reductively in each case by subsequently decreasing the potential to progressively lower values. Selected members of these negative- as well as positive-going segments are therefore shown in each figure. As is well-known,[1] the potential-dependent anodic formation and cathodic removal steps incur hysteresis arising from the activated nature of the process (vide infra).

The acquisition of the metal−gas SER spectra, shown for each metal alongside its electrochemical partner (Figures 1B−5B), followed a somewhat analogous protocol. The spectra were obtained upon heating the initially clean surface of each metal (vide infra) in a stepwise manner (mostly in 50 °C increments) to the temperatures indicated in 1 atm of flowing (100 cm^3 min^{-1}) dry O_2. Typically, 2 min was spent at each temperature. The highest temperature shown (300−400 °C) was determined by the emergence of stable oxide vibrational features (and limited to some extent by the need to retain SERS activity), followed by returning to 25 °C. The spectra are again stacked vertically upward in time in each case.

The SERS metal−oxygen vibrational frequencies obtained for each electrochemical and metal−gas system examined here are summarized in Table 1, along with corresponding literature Raman spectra for candidate bulk-phase metal oxides. Also included for comparison are typical metal−oxygen stretching frequencies for *adsorbed* atomic oxygen on single-crystal Pt-group surfaces, obtained by means of electron energy loss spectroscopy (EELS).

At least two overall features of these comparative data in Figures 1−5 are of particular interest here and therefore are emphasized in the specific descriptions for each system given below. First, the vibrational fingerprint yields insight into the structure as well as stability of each metal oxide, including a comparison of the nature of oxides formed in the electrochemical and gaseous environments. A second important property concerns the temperature at which thermal oxidation is achieved on the five metals, especially in relation to the potential-dependent onset of electrochemical oxidation/reduction at room temperature.

Electrochemical Oxidation. Figure 1A shows typical potential-dependent spectra obtained during the electrochemical oxidation of a platinum film in 0.1 M $HClO_4$. Increasing the potential to 0.8 V yields a broad band at 575 cm^{-1}, which increases in intensity at 1.0 V. Subsequently decreasing the potential negative of 0.6 V attenuates this feature, being removed below 0.4 V (Figure 1A). The hysterestic band intensity−potential dependence is consistent with cyclic voltammetry on such films, which exhibits broad anodic oxidation waves commencing at ca. 0.6 V and a well-defined oxide reduction peak at ca. 0.4 V.[3b] This voltammetric−spectral correlation provides clear evidence that the 575 cm^{-1} band arises from a metal−oxygen stretch due to a platinum oxide-type species. Similar SER spectra were reported earlier for Pt electrooxidation,[3b] although the low-frequency feature at 335 cm^{-1} is not seen here. (We suspect that this band arose from chloride contamination; vide infra.) While it is difficult to deduce the extent of surface oxidation from the vibrational data, it is well-known from the faradaic charge contained in the voltammograms that the oxide is on average only ca. 1−3 monolayers thick.[1] A similar situation applies to the other electrochemical oxides considered below.

Additional experiments using deuterated 0.1 M $HClO_4$ were performed to distinguish between oxide and hydroxide species. This tactic exploits the expected red shift of the related band when the latter, but not the former, species is present.[3a,b] The observed ca. 20 cm^{-1} red shift shows that the 575 cm^{-1} band involves a Pt−OH (or "hydrated" Pt−O) rather than Pt−O stretch (cf. ref 3b). This finding is in harmony with earlier in situ infrared results (in the O−H stretching region)[23] as well as the interpretation of electrochemical measurements.[1,24] Nonetheless, the appearance of the 575 cm^{-1} SERS feature resembles a published Raman spectrum of an amorphous PtO film and possibly PtO_2 (Table 1).[18]

A similar series of potential-dependent SER spectra for palladium in 0.1 M $HClO_4$ is displayed in Figure 2A. While the spectra obtained up to 0.6 V are largely featureless, surface oxidation is evident by 0.8 V from the appearance of a SERS band at 530 cm^{-1}, which grows markedly by 1.0 V. During the negative-going potential segment, the 530 cm^{-1} band attenuates and finally disappears by 0.4 V, again in harmony with the corresponding voltammetric data that show an oxide reduction peak at ca. 0.45 V. No red shift of the 530 cm^{-1} peak was discerned upon solvent deuteration, indicating the presence of a palladium oxide rather than hydroxide species. However, no clear-cut assignment of this feature to a stoichiometric Pd oxide can be made upon comparison with bulk-phase spectra. The SERS band differs markedly from that of well-characterized PdO, which exhibits Raman features at 445 and 650 cm^{-1} (Table 1).[19] Although it has been reported that a PdO_3 species gives rise to a similar infrared band at ca. 530 cm^{-1},[25] the existence of this moiety is uncertain.

Corresponding SER spectra obtained for the electrochemical oxidation of iridium are displayed in Figure 3A (cf. ref 3d).

Since the as-deposited iridium film contained some oxide upon SERS inspection, the electrode was subjected to cathodic H_2 evolution at −0.4 V before returning to 0 V (bottom spectrum). However, a weak yet sharp SERS band at ca. 580 cm^{-1} is still evident. When the potential is raised to 0.6 V, a broad SERS feature is observed at 530 cm^{-1}, which maintains a similar intensity up to 1.0 V. During the subsequent negative-going potential segment, an additional band at 315 cm^{-1} is discerned at 0.4 V. The 530 cm^{-1} band starts to attenuate by 0.2 V, and finally disappears at 0 V, the 580 cm^{-1} SERS feature reappearing at this point. Solvent deuteration yields a significant 530 cm^{-1} band red shift, again ca. 20 cm^{-1}, indicating the presence of an Ir−OH vibration. However, the 580 cm^{-1} band is insensitive toward solvent deuteration.[3d]

It is well-known that the surface electrochemistry of iridium behaves somewhat differently than other Pt-group metals in that its oxide is irreducible under certain conditions.[26,27] This is apparently manifested here by the survival of the 580 cm^{-1} band even into the cathodic hydrogen evolution region. Recently, we have reported that this unusually stable species, attributed to crystalline IrO_2 (Table 1), can be formed readily in NO-saturated 0.1 M $HClO_4$.[3d] However, the assignment of the broader 530 cm^{-1} band is uncertain; there is no literature vibrational spectrum of iridium hydroxide for comparison.

Representative potential-dependent SER spectra for rhodium in 0.1 M $HClO_4$ are shown in Figure 4A. When the potential is raised to 0.6 V, a SERS peak appears at 540 cm^{-1}, its intensity increasing up to 1.0 V. No observable change in the SER spectra is discerned during the negative-going potential segment down to 0.2 V, but the 540 cm^{-1} band essentially disappears by 0 V, again in harmony with the corresponding voltammogram that shows a broad oxide reduction peak at ca. 0.1 V. This SERS feature is tentatively assigned to Rh_2O_3, since it has a comparable appearance to the corresponding SER spectrum formed in dry O_2, known to arise chiefly from this species (Figure 4B, vide infra).[5b]

Lastly, potential-dependent SER spectra for electrochemical oxidation of ruthenium are displayed in Figure 5A (cf. ref 5e). When the potential is increased to 0.6 V, a weak SERS band at 480 cm^{-1} is observed, which develops at 0.8 V along with an additional band at 710 cm^{-1}. The reversal potential was set at 0.8 V (rather than 1.0 V as above) since it is known that at more positive values the Ru surface undergoes corrosion.[28] During the negative-going potential excursion, the 710 cm^{-1} band disappears below 0.4 V, while the 480 cm^{-1} feature survives until ca. −0.2 V. A band also appears at 610 cm^{-1} from +0.2 to −0.2 V. A near-reduced surface was only achieved when the potential was lowered to the hydrogen evolution region, −0.4 V. Solvent deuteration did not yield significant band red shifts, indicating that ruthenium oxides rather than hydroxides are involved.[3b] As discussed in our earlier study,[5e] the 480 and 710 cm^{-1} bands are assigned to different stretching modes of RuO_2 (Table 1). However, no clear SERS evidence of higher ruthenium oxides such as RuO_4 is discernible, not surprisingly, in view of the anticipated dissolution of such species at high potentials.[28]

Although the precise nature of the surface oxide formed electrochemically is in most cases uncertain, it is of interest to examine the electrode potential, E_i, at which surface oxidation initially occurs for each metal, as prescribed by the initial appearance/removal of the SERS features, in relation to the equilibrium formation potentials of likely bulk-phase oxides, E_{eq}. This comparison is given in Table 2. The E_{eq} values were obtained from literature standard free energies of formation, ΔG_f°, for the oxides listed, by means of

$$E_{eq} = E^\circ(O_2) + \Delta G_f^\circ/nF \quad (1)$$

where n is the number of electrons required to form the oxide from water electrooxidation, F is the Faraday constant, and $E^\circ(O_2)$ is the reversible oxygen electrode potential (equal to 0.93 V vs SCE at pH 1). Note that the ΔG_f° and hence E_{eq} values given for "PtO" are distinctly uncertain (see ref 29). The E_i values were obtained from the mean of the potentials where the oxide SERS band is discerned to initially form and subsequently be removed during suitably slow positive- and negative-going potential excursions, respectively. This procedure is, of course, inherently approximate (± 0.1 V) given the substantial hysteresis, not to mention the uncertain composition of the electrochemical oxides. Nevertheless, the reasonable concordance observed between E_{eq} and E_i, including the affinity order Pt ∼ Pd < Ir ≤ Rh < Ru predicted from the oxide formation thermodynamics, is reproduced well by the SERS data. The significance of this trend in relation to the behavior of the thermal oxidation processes is considered below.

TABLE 2: Comparison between Measured Initial Potentials for Surface Electrochemical Oxidation and Predicted Bulk-Phase Equilibrium Values

metal[a]	oxide[b]	$-\Delta G_f^\circ$ [c] (kcal/mol)	E_{eq} [d] (V)	E_i [e] (V)
Pt	PtO	∼15[f]	∼0.6	0.6
Pd	PdO	20[g]	0.50	0.6
Ir	IrO_2	45[h]	0.45	0.4
Rh	Rh_2O_3	70[i]	0.43	0.3
Ru	RuO_2	60[f]	0.28	0.2
	RuO_4	36[k]	0.75	

[a] Metal surface examined here. [b] Oxide suggested to be formed (may be related hydrated/hydroxide; see text). [c] Standard free energy of formation of oxides, from references given. [d] Equilibrium potential (V vs SCE) for electrochemical oxide formation at pH 1, from eq 1 and ΔG_f° values listed. [e] Initial potential for electrochemical surface oxidation at pH 1, largely from SERS data (see text). [f] See discussion in ref 29. [g] Reference 30. [h] Reference 31. [i] Reference 31a. [j] Reference 32. [k] Reference 33.

Thermal Oxidation. We now turn to describing the temperature-dependent SER spectra formed on each metal, along with comments concerning previous reports of surface oxidation in high-pressure O_2 environments. The more extensive literature referring to UHV conditions is considered separately below. It is important at the outset to recognize the thermodynamic as well as kinetic differences between such "higher-pressure" and "UHV-like" reaction conditions. While the ΔG_f° values for each of the metal oxides considered here are negative at room temperature (Table 2), these of course refer to 1 atm of O_2. Increasing the temperature, to surmount an activation barrier to surface oxide formation (vide infra), and/or lowering the O_2 pressure, will mitigate against the oxide thermodynamic stability. As is well-known,[37] the "dissociation pressure" of platinum oxide, in particular, is sufficiently large to thermodynamically prohibit at least bulk-phase oxidation unless higher O_2 pressures (e.g., $>10^{-2}$ Torr) are employed. The greater stability (i.e., more negative ΔG_f° values) of the Pd, Ir, Rh, and Ru oxides considered here does make it thermodynamically *feasible* that metal oxidation can proceed even at elevated temperatures and with the O_2 dosing pressures (e.g., $\leq 10^{-6}$ Torr) typically employed in UHV-based experiments. However, kinetic factors can, and probably do, trigger markedly different surface chemistry compared to the ambient-pressure O_2 conditions considered here.

Before the samples were subjected to thermal oxidation in flowing oxygen, following rinsing and transfer from the electrodeposition cell to the gas-phase chamber, some pretreatment was required to obtain a clean surface as gleaned by featureless SER spectra. Platinum and palladium films were heated in 1 atm of H_2 to 150 °C in order to remove residual adsorbed chlorine from the deposition bath, appearing as a metal−adsorbate stretching band around 270−330 cm^{-1}.[34] For rhodium, and especially iridium and ruthenium, initial SERS inspection revealed that the transferred films usually contain surface oxide bands, formed during transfer through air. Since O_2-induced oxidation requires elevated temperatures (vide infra), we believe that the oxide is produced by an "electrochemical"-like process involving water as well as O_2. Briefly, the surface potential is increased as a result of oxygen reduction at the wet metal-air interface, up to a value where electrochemical oxide formation (from water) is thermodynamically favorable. This explanation is supported by the observation that the more noble surfaces (platinum and palladium) are invulnerable to such "electrochemical oxidation" in air, largely because their equilibrium potentials for oxidation are higher (Table 2). We have previously described similar "electrochemical" reactions to account for surface oxide chemistry at other metal−wet gaseous interfaces.[35,36]

While this adventitious rhodium oxide can readily be reduced thermally in H_2 at 150 °C,[5h] such a pretreatment was less applicable to iridium and ruthenium since higher reduction temperatures were required, potentially degrading the SERS activity. We therefore utilized an alternative pretreatment that involves exposure to CO-saturated 0.1 M $HClO_4$ at −0.3 V, emersion with potential control and transfer to the gas-phase reactor with the CO acting as a protective adlayer,[5e] and then desorbing the CO at 200 °C. Following the above pretreatments for each metal, initial exposure to dry oxygen as well as argon at room temperature yielded featureless spectra in the frequency range 200−3000 cm^{-1}. It is important to note that no carbonaceous bands, usually observed in the 1300−1600 cm^{-1} range, were evident at any temperature in the presence of oxygen, although such features could be formed upon heating the present surfaces in nonoxidizing gaseous environments.

Figure 1B displays a typical set of temperature-dependent SER spectra for platinum to 1 atm of flowing O_2. The spectra are stacked from bottom to top with increasing time. Inspection of Figure 1A reveals essentially featureless spectra up to 150 °C; the emergence of a broad SERS feature centered at 575 cm^{-1} is only seen for $T \geq 200$ °C. A weaker feature at ca. 825 cm^{-1} appears at 300 °C, and both bands remain intact upon subsequent cooling back to 25 °C. The 575 cm^{-1} band is assigned to "amorphous" PtO on the basis of its similarity with the reported normal Raman spectrum (Table 1).[18] The identity of the additional SERS feature at ca. 825 cm^{-1} detected at 300 °C is uncertain; it may arise from a higher Pt oxide such as PtO_2.[18]

Unlike the present in situ SERS approach, the literature studies referring to higher O_2 pressures chiefly involve ex situ transfer strategies. For example, X-ray photoelectron spectroscopy (XPS) revealed that heating Pt(111) in 1 atm O_2 to 600 °C produced about two monolayers of PtO_2.[38] (As is well-known, XPS is able to distinguish such oxide species from adsorbed atomic oxygen through their characteristic O(1s) binding energies.) Another study deduced that platinum starts to oxidize at ca. 450 °C under ambient O_2 by measuring the increase in electrical resistance of a Pt film.[39]

Figure 2B displays temperature-dependent SER spectra obtained for the thermal oxidation of palladium in 1 atm flowing O_2. Again, no detectable SERS features are discernible upon initial oxygen exposure at 25 °C or even up to 150 °C. Upon increasing the temperature to 200 °C, however, a pair of SERS bands appear at 445 and 670 cm^{-1}, which are stable at least up to 300 °C and after returning to 25 °C (Figure 2B). The assignment of these SERS features is facilitated upon comparison with Raman spectra of model stoichiometric oxides (Table 1). The 445 and 670 cm^{-1} SERS bands are both assigned to PdO from their similarity to spectra observed for PdO formed on an oxidized Pd foil.[19a] Interestingly, the SER spectra for this thermally oxidized palladium (Figure 2B) are quite different from that for the electrochemical surface oxide (Figure 2A). The close correspondence of the former, but not the latter, to the PdO spectral fingerprint suggests that the elevated temperature condition yields a more "crystalline" oxide, with better-developed phonon properties.

Several higher-pressure studies on palladium oxidation have been documented. For example, the formation of PdO has been deduced by XPS upon heating a polycrystalline Pd surface in air to 600 °C or higher.[40] A more recent study has also utilized XPS to identify an intricate O_2 pressure-dependent formation of surface PdO at 150 °C on Pd(110).[41] Ellipsometry along with XPS and Auger electron spectroscopy (AES) have shown that the onset of oxide formation on Pd(111) and polycrystalline Pd occurs at ca. 200 °C at O_2 pressures up to ca. 10^{-2} Torr.[42] As for Pt, then, the available literature supports the present deduction from SERS that elevated temperatures are required to form surface oxide on palladium even at ambient O_2 pressures.

Typical temperature-dependent SER spectra acquired for the thermal oxidation of iridium are displayed in Figure 3B. (Note that we have selected a spectral set exhibiting an initially reduced surface, as gleaned partly from the absence of the 580 cm^{-1} feature evident in the electrochemical data set, Figure 3A. However, some gas-phase experiments also show this sharp band prior to heating in O_2.) Again, no detectable SERS feature was observed upon initial oxygen exposure (bottom spectrum) to the reduced surface. When the temperature was raised only moderately, to 100 °C, however, a broad SERS band centered at ca. 540 cm^{-1} evolved, which developed further toward higher temperatures and after cooling back to 25 °C. This feature is tentatively assigned to "amorphous" IrO_2; its peak frequency is in reasonable agreement with the major Raman band for crystalline IrO_2, although the former is much broader. Little has been reported previously regarding iridium surface oxidation at higher oxygen pressures. One study using XPS and EELS claimed that heating Ir(111) in 1 atm O_2 at 600 °C yielded a surface oxide that was, however, distinguishable from bulk-like IrO_2.[43]

Figure 4B displays temperature-dependent SER spectra obtained for rhodium exposed to 1 atm oxygen. We have discussed this system previously by means of combined in situ SERS and ex situ XPS measurements.[5b] Once again, the spectra remained featureless until 200 °C, a broad SERS band peaked at 540 cm^{-1} then being detected. The band develops slightly toward higher temperatures and remains upon returning to 25 °C. This feature has been previously assigned to Rh_2O_3 as facilitated by XPS as well as comparison with the Raman spectra of model compounds (Table 1).[5b] The present data (Figure 4B), however, do not show the band at 290 cm^{-1} reported earlier.[5b] We suspect that this feature was due to contamination from adsorbed chloride, the improved "pinhole-free" Rh overlayers

used in the present study eliminating chlorine emanating from the underlying SERS-active gold template. The close resemblance of the electrochemically and thermally formed oxide bands on rhodium (Figure 4A, B) indicate that the surface structures are similar. The growth of surface oxide on rhodium at higher O_2 pressures has also been examined by atom-probe mass spectrometry and field ion microscopy, showing that Rh_2O_3 only formed at elevated temperatures, ca. 250 °C, at O_2 pressures above 0.01 Torr.[44] On the other hand, heating Rh(111) in 1 Torr O_2 yielded oxide with lower O/Rh ratios than Rh_2O_3, as deduced from AES.[45]

As for rhodium, we have previously used SERS and XPS to investigate the progressive thermal oxidation of ruthenium.[5e] Unlike the corresponding electrochemical system noted above, the multiple ruthenium oxide stoichiometries anticipated from the bulk-phase chemistry are evident in the ambient-pressure gas-phase system. Figure 5B displays typical temperature-dependent SER spectra for ruthenium exposed to 1 atm O_2. Despite the high affinity of Ru for oxygen, as for the other surfaces, no SERS features appeared until heating. By 200 °C, several SERS bands became discernible at 470, 620, and 800 cm^{-1}. The 620 cm^{-1} band, however, disappeared at 250 °C along with the advent of a new feature at 875 cm^{-1}.[5e]

The SER spectral interpretation has been aided by parallel XPS measurements as well as comparisons with Raman spectra of model ruthenium oxides.[5e] The SERS bands at 470/620, 800, and 875 cm^{-1} have thereby been assigned to RuO_2, RuO_3, and RuO_4, respectively (Table 1). The temperature-dependent data therefore imply that RuO_2 and RuO_3 are produced at 200 °C, more oxygen being incorporated into the film at 250 °C to favor the presence of RuO_4. However, when the temperature was decreased to 25 °C, RuO_2 and RuO_3 re-form at the expense of RuO_4, presumably by decomposition of the latter.[5e]

We have so far considered only surface oxide, rather than adsorbed oxygen, implying that the oxygen is incorporated into the metal substrate and, presumably, forms a coherent lattice oxide structure, thereby exhibiting phonon vibrational modes. This is perhaps most clearly the case for the electrochemical systems, where the potential-dependent hysterestic correlation evident between the voltammetric and SERS data diagnoses the presence of oxide rather than adsorbed O/OH since only the former process is nonreversible.[1] Somewhat analogously, the marked thermal activation required for the gas-phase O_2 oxidation also prescribes the SER spectra as arising from oxide rather than adsorbed atomic oxygen, since the latter species are readily formed upon O_2 dosing even at subambient temperatures.[46]

Nonetheless, it is appropriate to consider if adsorbed oxygen in the present systems should be detected by SERS. Table 1 contains representative metal−O vibrational frequencies, υ_{M-O}, for adsorbed atomic oxygen, O_{ad}, formed chiefly on hexagonal metal surfaces in UHV, as measured by EELS. It should be borne in mind that the frequencies are sensitive to the coordination geometry, as exemplified by the lower υ_{M-O} value seen on Rh(100) versus Rh(111).[47] The absence of discernible SERS bands at near-ambient temperatures (in gaseous O_2) at these characteristic υ_{M-O} frequencies, 400−500 cm^{-1}, is perhaps surprising, given the likely presence of O_{ad} under these conditions.[46] Most likely, this reflects weak Raman scattering for adsorbed oxygen, mitigating against its detection. Evidence favoring this notion is evident from the observation of only a weak SERS band at 570 cm^{-1} upon dissociative NO chemisorption on palladium at 25 °C, probably due to adsorbed oxygen (cf. ref 49), along with a much stronger 300 cm^{-1} feature attributable to a comparable coverage of adsorbed atomic nitrogen.[5d] Heating this surface to above 200 °C yields bands at 665 and 450 cm^{-1}, similar to Figure 2B, again indicative of PdO formation.[5d]

Related Studies in Ultrahigh Vacuum. Given that the electrochemical surface oxidation of all five metals considered here can be triggered at room temperature at electrode potentials close to (within ca. 0.2−0.3 V of) the thermodynamic values, the above observation that ambient-pressure O_2 thermal oxidation is initiated only at elevated temperatures is at first sight surprising. An examination of selected UHV-based systems, however, supports this qualitative deduction. We now summarize briefly some salient UHV-based findings, emphasizing the conversion between adsorbed and "subsurface" atomic oxygen. The latter species is in principle the precursor to the "surface oxide" of interest here, even though UHV-like conditions are not usually conducive to full development of the latter phase (vide infra).

While clear-cut detection of subsurface oxygen is often not straightforward, work-function (Φ) measurements have proved to be a sensitive means of following the "adsorbate to subsurface" conversion, $O_{ad} \rightarrow O_{ss}$, both as a function of temperature and oxygen dosage or pressure.[41,50−52] While O_{ad} yields substantial ($\geq$0.5 eV) Φ increases due to the "outward-pointing" surface dipole, O_{ss} exhibits instead Φ *decreases*, reflecting a dipole reversal.[50a,51] [Interest in this phenomenon has been heightened by its utilization in the photoemission electron microscope (PEEM), enabling local adsorbate imaging.[50]] Heating Pt(100) dosed with O_{ad} patches above ca. 180 °C initiates production of O_{ss} on this basis, which is complete by 380 °C.[50b] Conventional Φ measurements have also been used to probe thermally induced $O_{ad} \rightarrow O_{ss}$ conversions, for example, on Ir(110).[52] Observing the $O_{ad} \rightarrow O_{ss}$ transition by this means by varying the O_2 exposure at a given temperature is problematic, although nonmonotonic $\Delta\Phi$−exposure plots have been obtained even at room temperature on Pd(110), suggestive of some O_{ss} production.[41]

Evidence for the requirement of elevated temperatures to achieve substantial $O_{ad} \rightarrow O_{ss}$ conversion by O_2 dosing on Pt-group metals has been gleaned from several other UHV-based measurements, especially AES, XPS, and EELS. For example, the last technique has been used to deduce an $O_{ad} \rightarrow O_{ss}$ conversion on the stepped surface Pd(112) upon heating to ca. 250 °C.[49] Interestingly, this transformation did not occur on Pd(111),[49] reflecting the often-observed facilitation of O_{ss} and eventual oxide production by surface steps and defects.[2]

As already mentioned, a chronic limitation to UHV-based examinations of surface oxidation is the relative inability of dioxygen to act as a thermodynamically and kinetically facile oxidant, except at higher pressures. A means of circumventing this problem, which has received increasing attention recently, is to utilize better "O-donor" oxidants, such as O_3 and NO_2.[53−56] These species can yield very high O_{ad} coverages even under UHV dosing conditions, a condition achieved with O_2 only with difficulty at much higher pressures. Indeed, the formation of "surface oxide" on Pt(111) even at room temperature upon ozone dosing was deduced from AES and temperature-programmed desorption (TPD) measurements.[53b] This study highlights the importance of attaining high O_{ad} packing densities in triggering the $O_{ad} \rightarrow O_{ss}$ conversion in addition to the desirability of elevated temperatures to surmount the kinetic barrier.

Interestingly, however, while NO_2 dosing on Pt(111) at 130 °C yields relatively high O_{ad} coverages, 0.75, there is no evidence for oxide formation up to the desorption temperature.

On the other hand, NO_2 dosing at elevated temperatures on Pd(111) yields O_{ss} and possibly oxide, on the basis of XPS, reflecting the higher oxygen affinity of Pd relative to Pt.[54b] The $O_{ad} \rightarrow O_{ss}$ conversion has also been observed on Rh(111) dosed with NO_2 upon heating above 100 °C.[55] Last, the sequential surface oxidation of Ru(001) induced by NO_2 exposure above ca. 300 °C has recently been examined.[56] The transition between O_{ss}, the early stages of oxidation ("RuO_x" formation)[56a] and even the formation of higher oxides (RuO_3, RuO_4) at large exposures and temperatures[56b] has been identified by TPD, EELS, and XPS. These observations are compatible with the temperature-dependent oxidation of ruthenium by ambient-pressure O_2, as seen here by SERS (Figure 5B).

Comparison between Electrochemical and Gas-Phase Surface Oxidation. The foregoing SERS data, summarized in Figures 1−5, show that while the *nature* of the oxide films formed on Pt-group metals in aqueous electrochemical and ambient-pressure O_2 environments displays overall similarities, the conditions necessary to induce such surface oxidation are remarkably dissimilar. First, while the electrochemical films are formed readily at room temperature, oxidation by ambient-pressure dry O_2 *uniformly* requires elevated temperatures, in most cases 200 °C or above. Second, while the electrode potentials at which electrooxidation is initiated vary approximately with the metal oxide thermodynamic stabilities, no related correlation is evident in the temperature-dependent O_2 oxidation.

Furthermore, the electrochemical oxidations proceed upon applying only modest anodic overpotentials (i.e., small free-energy driving forces). More specifically, the net electrode process

$$M + H_2O - 2e^- - 2H^+ \rightarrow MO \qquad (2)$$

where M and MO are the reduced metal and metal oxide, respectively, can be induced to occur at 25 °C by applying small (ca. 0.2−0.3 V) driving forces above the equilibrium potential value, E_{eq}, where by definition the "half-reaction" free energy $\Delta G_e^\circ = 0$. These overpotentials are equivalent to $-\Delta G_f^\circ$ values of ca. 5−15 kcal mol^{-1}, from eq 1. The "thermal chemical" reactions

$$M + {}^1/_2O_2 \rightarrow MO \qquad (3)$$

on the other hand, necessarily involve *larger* $-\Delta G_f^\circ$ values, 15−70 kcal mol^{-1} (Table 2). The more thermodynamically favorable nature of the latter processes can also be quoted in "overpotential" parlance via eq 1, being equal to $[E^\circ(O_2) - E_{eq}]$, i.e., ca. 0.35−0.65 V (Table 2). Consequently, the relative driving forces for the gaseous O_2 versus aqueous oxidation pathways are given by the reversible redox potential for the O_2/H_2O couple, $E(O_2)$, in relation to the applied electrode potential, E_{app}, for the electrochemical route. At least for the conditions considered here, ambient-pressure O_2 and acidic aqueous solutions, $E(O_2) > E_{app}$, the inequality being ca. 0.2−0.4 V. The higher temperatures required for the 1 atm O_2 gas-phase oxidations are therefore notable given this energetic advantage over the electrochemical processes. Couched in such terms, then, the different chemical kinetics displayed by the electrochemical and gas-phase oxidations clearly indicate the occurrence of *intrinsically* more facile reaction pathways in the former case. We now consider the likely kinetic factors responsible for this notable disparity.

The most obvious difference between the nature of the electrochemical and gas-phase surface oxidation is that the former involves charge transfer driven by a variable (and controllable) surface potential, and hence electrostatic field; the latter oxygen adsorption/incorporation processes entails no coupled redox step, even though field-dependent charge motion also occurs. These differences are intimately associated with the nature of the water and dioxygen O_{ad} sources. The aqueous double-layer environment provides a constant "saturated coverage" of H_2O, from which the reactive chemisorbates OH_{ad} and O_{ad} are readily formed by coupled electron−proton transfer. While the coverages of the latter species formed prior to surface electrooxidation are not well-known for most systems, their reversible potential-dependent formation has been demonstrated clearly from conventional electrochemical measurements.[1] As expected from eq 1, increasing the pH shifts the potential region where OH_{ad}/O_{ad} and surface oxide forms to lower values, reflecting the proton transfer.[1] One can therefore visualize the aqueous interface as providing a highly variable/controllable source, depending on the applied potential and solution pH, of atomic oxygen/hydroxyl, which forms the active surface oxidant.

The gaseous dioxygen environment provides atomic oxygen via dissociative chemisorption. However, the efficiency of the dissociative binding pathway, and thereby the effective steady-state O_{ad} coverages, can be inhibited by the need for "open" adsorption sites as well as by the reaction energetics. Consequently, the O_{ad} coverages usually formed, for example, on Pt(111) by O_2 dosing are relatively low, 0.25, even though larger values can be attained at moderate pressures and higher temperatures.[57,58] Unfortunately, however, little is known concerning the actual O_{ad} coverages present at the high O_2 pressures of interest here. It is therefore unclear if the need for elevated temperatures to achieve O_2-induced surface oxidation is connected with enhanced coverages of the O_{ad} precursor, or if other factors are responsible (vide infra).

An advantageous property enjoyed by the electrochemical system is that oxygen incorporation into the metal lattice can be assisted by the adjustable electrostatic field at the metal−solution interface. Increasing the surface potential will favor this process since it involves motion of electronegative species ($O^{\delta-}$) toward/into the metal surface, akin to oxidative electron transfer. The notion of such "high-field assisted ion transport"[59] is indeed analogous to interfacial charge transfer and can be applied formally even to the initial monolayer stage of film growth on noble metals.[60] One could therefore surmise that the room-temperature oxidation of Pt-group metals in aqueous solution is facilitated by the high electrode potentials acting to lower the barrier to oxygen incorporation into the metal lattice.[60] The need for elevated temperatures in the O_2-induced gas-phase oxidation could then be attributed to the absence of such favorable electrostatic fields at the electrically neutral metal−gas interface, necessitating an alternative thermally driven $O_{ad} \rightarrow O_{ss}$ conversion.

Comparison of the likely surface potentials characterizing the electrochemical and metal−gas considered here, however, does not support this hypothesis. The electrode potential, E, for a given electrochemical interface can be related to the work function, Φ, of a similar metal−vacuum (or metal−gas) interface by[61,64]

$$E = \Phi/e - E_{ref}(ab) \qquad (4)$$

where e is the electron charge and $E_{ref}(ab)$ is the so-called "absolute potential" of the reference electrode. (The latter term converts electrode potentials to the "vacuum reference" scale obliged for Φ measurements.) The appropriate values of $E_{ref}(ab)$ remain somewhat uncertain, estimates for the standard

hydrogen electrode (SHE) around 4.5 and 4.8 V being deduced by different means.[62] An estimate close to the latter value, however, has been deduced from analysis of surface potential-dependent stretching frequencies for chemisorbed CO and NO at Pt-group metal−aqueous compared with metal−UHV interfaces.[63,64] This estimate transposed to the SCE scale employed here yields $E_{ref}(ab) \sim 5.0$ V. Taking Pt(111) as an example, the work function of the clean surface is 5.9 eV.[65] Binding atomic oxygen increases Φ substantially on this and other Pt-group surfaces; for example, $\Delta\Phi = 0.35$ eV at $O_{ad} = 0.5$,[54a] yielding $\Phi = 6.25$ eV. While no oxide, or apparently even O_{ss}, forms under these conditions on Pt(111) at 130 °C,[54a] this surface potential is equivalent to $E \sim 1.2$ V vs SCE from eq 4.

However, it is well-known that electrochemical Pt surface oxidation, even in acidic media, commences at substantially *lower* surface potentials; thus the SER spectra obtained for Pt in 0.1 M $HClO_4$ show oxide formation by 0.8 V vs SCE (Figure 1A). Similar findings also apply to other Pt-group surfaces. Indeed, the surface potentials attained at the metal−gas interfaces, especially in the presence of adsorbed oxygen, are usually higher than the corresponding values attained at the metal−aqueous interfaces where surface oxidation readily proceeds. Although additional contributions to the surface potentials for the metal−solution systems arise from solvent and free ionic/electronic charge, the net electrostatic fields present at the metal−gas interfaces should favor oxygen charge transport into the metal to a comparable or even greater extent than for the electrochemical case. This finding is also intuitively in harmony with the above deduction of greater chemical driving forces for the gas-phase relative to the electrochemical surface oxidation.

Most likely, then, the markedly more facile kinetics associated with the electrochemical metal oxidation arise from the availability of a different oxygen incorporation pathway at the metal−solution interface. The usual model considered for gaseous/UHV systems in the literature involves the formation of subsurface oxygen, O_{ss}, as already noted, followed (in energetically favorable cases) by the development of a coherent metal oxide "surface phase". Evidence for the $O_{ad} \rightarrow O_{ss}$ conversion, such as from work-function measurements, has already been noted. One apparent uncertainty concerns the typical stability of the O_{ss} versus O_{ad} states. Thus kinetic studies of the conversion on Rh(111) at $T > 100$ °C indicate a significant (4.5 kcal mol^{-1}) barrier due chiefly to the lower stability of O_{ss}.[55] On the other hand, the complete thermal-induced conversion of O_{ad} to O_{ss} on Pt(100) observed by PEEM at $T \geq 300$ °C indicates that the latter state is more stable, albeit involving a substantial (ca. 15 kcal mol^{-1}) barrier to its formation from O_{ad}.[50b] While the microscopic nature of the $O_{ad} \rightarrow O_{ss}$ conversion undoubtedly depends on the metal substrate, being affected greatly, for example, by surface defect and other crystallographic factors,[2] the qualitative picture involves an intimate coupling between oxygen adsorption, penetration, and metal lattice fluctuations.[66] High O_{ad} coverages are anticipated to facilitate the required metal lattice distortions;[66] indeed, direct evidence for adsorbate-induced Pt(111) phonon "softening" under these conditions has been obtained.[58] The abundant presence of the O_{ad} precursor species is therefore conducive to, and possibly even a prerequisite for, the occurrence of the $O_{ad} \rightarrow O_{ss}$ conversion at metal−gas interfaces.

The nature of oxygen atom lattice incorporation at metal−solution interfaces, however, is seemingly quite different. The traditional picture of the initial stages of surface oxidation involves metal−oxygen "place exchange", whereby the O_{ad}/OH_{ad} species switches positions with a surface metal atom, the latter thereby occupying an "adatom" position.[1] Intriguingly, recent ex situ X-ray scattering measurements for Pt(111)−aqueous interfaces substantiate this notion, showing the extensive formation of Pt adatoms above the (111) lattice plane.[67] Some related information has been obtained for anodic oxide formation at gold−aqueous interfaces by in situ scanning tunneling microscopy (STM).[68] A key feature of the place-exchange mechanism is that the metal adatoms so produced should carry a partial positive charge, that is, undergo ionization similarly to the metal oxide state. In the gas phase, this process will be disfavored by the loss of metal−metal cohesive energy, albeit offset by metal oxide lattice stabilization. However, in the electrochemical environment such partial metal ionization will be stabilized considerably by the interfacial solvent. Indeed, the redox potentials $E(M^{n+})$ for forming bulk-phase solvated cations M^{n+} from the solid metals are only slightly higher than for the formation of metal oxides in the acidic solution employed here. For example, $E(M^{n+}) \sim 0.95$, 0.67, and 0.45 V vs SCE for forming Pt^{2+}, Pd^{2+}, and Rh^{3+}, respectively.[69] Note that these potentials are close to the E_{eq} values in pH 1 for forming the corresponding oxides (Table 2); indeed, dissolution of the noble metal in this fashion (i.e., metal corrosion) is usually only prevented by the passivating effect of the oxide layers, along with electrode kinetic factors. Consequently, the place-exchange pathway, probably yielding growing patches of oxide nucleated directly by this means, can be envisaged to be facilitated substantially by interfacial solvation at the electrochemical interface.

Indeed, any such mechanism that involves interfacial charge formation/separation, such as $M^{\delta+}-O^{\delta-}$ moieties, will be stabilized by the presence of an ionic solvating medium.[70] In the gas-phase/vacuum environment, the absence of such dielectric stabilization could therefore necessitate oxide production to occur via an intermediate O_{ss} state, where the oxygen atoms are incorporated first into the metal lattice *without* metal adatom formation, at least in a partially cationic state. Formation of the metal oxide surface phase would therefore occur by suitable "agglomeration" of subsurface oxygen into a coherent ionic lattice. Admittedly, these notions are somewhat speculative; the difficulty in oxidizing noble metal surfaces in conventional UHV environments leads to a paucity of microscopic structural information, even in relation to that available for in situ electrochemical systems. However, at least on a qualitative level this mechanistic picture can account for the remarkably more facile Pt-group metal oxidations observed in the electrochemical versus the ambient-pressure O_2 environment.

Concluding Remarks

While the limitation of the present SERS strategy to polycrystalline transition-metal surfaces does constitute a restriction from a "fundamental surface science" perspective, its major virtue here is to enable a surface chemical process of importance to both electrochemical and gaseous-phase systems to be examined in a uniquely unified fashion. The notable more facile surface oxidations evident in the gaseous electrochemical environments reflect an intrinsically greater potency of water as a metal oxidant in comparison with dioxygen. The need for substantially elevated temperatures to trigger surface oxidation in dry O_2, even on metals such as ruthenium having high oxygen affinities, might be viewed as surprising, at least to electrochemists or corrosion engineers familiar with the occurrence of these processes at ambient temperatures in aqueous solution or in wet air. While the requirement of elevated temperatures to induce Pt-group metal oxidation by dioxygen is consistent with literature findings, including UHV-based studies, the

precise factors responsible for the highly activated nature of these processes remain unclear. One probable factor is the difficulty of forming a suitable high coverage of chemisorbed atomic oxygen from dioxygen. The occurrence of ambient-temperature oxidation of Pt(111) upon ozone dosing, yielding monolayer levels of O_{ad}, favors this interpretation.[53b]

However, the remarkable efficacy of aqueous electrochemical oxidations, displaying partial thermodynamic control even at ambient temperatures, most likely arises from the occurrence of a fundamentally different oxide formation pathway. The facility of the well-documented metal−oxygen place-exchange mechanism, featuring the intermediate formation of metal adatoms, given its apparent absence (or at least ineffectiveness) in the gaseous environment, is most plausibly associated with interfacial solvation. Given these differences it would be of interest to scrutinize metal oxidations in wet O_2 environments, especially water vapor/O_2 gas mixtures. The close connection between metal oxidations in aqueous electrochemical and ambient air has recently been noted for copper.[35] Such a study for Pt-group metal oxidations is planned in our laboratory.

Along with infrared reflection−absorption spectroscopy (IRAS), then, SERS offers an increasingly versatile means of scrutinizing adsorption chemistry at electrochemical and other metal−ambient interfaces for which fundamental information has been largely lacking in comparison with metal−UHV systems.[71] As exemplified by the present study, such data can serve to highlight major differences as well as similarities in analogous surface chemistry occurring in solution and gas-phase environments.

Acknowledgment. This work has been supported by the National Science Foundation and the Petroleum Research Fund, with additional funding via a contract from the Hewlett-Packard Co.

References and Notes

(1) Conway, B. E. *Prog. Surf. Sci.* **1995**, *49*, 331.

(2) Brundle, C. R.; Broughton, J. Q. In *Chemisorption Systems*; King, D. A., Woodruff, D. P., Eds.; The Chemical Physics of Solid Surfaces and Heterogeneous Catalysis, Vol. 3A; Elsevier: Amstedam, 1990; Chapter 3.

(3) (a) Desilvestro, J.; Weaver, M. J. *J. Electroanal. Chem.* **1986**, *209*, 377. (b) Zhang, Y.; Gao, X.; Weaver, M. J. *J. Phys. Chem.* **1993**, *97*, 8656. (c) Chan, H. Y. H.; Takoudis, C. G.; Weaver, M. J. *J. Phys. Chem. B* **1999**, *103*, 357. (d) Zou, S.; Chan, H. Y. H.; Williams, C. T.; Weaver, M. J. *Langmuir*, in press.

(4) (a) Leung, L.-W. H.; Weaver, M. J. *J. Am. Chem. Soc.* **1987**, *109*, 5113. (b) Leung, L.-W. H.; Weaver, M. J. *Langmuir* **1988**, *4*, 1076.

(5) (a) Wilke, T.; Gao, X.; Takoudis, C. G.; Weaver, M. J. *Langmuir* **1991**, *7*, 714. (b) Tolia, A. A.; Smiley, R. J.; Delgass, W. N.; Takoudis, C. G.; Weaver, M. J. *J. Catal.* **1994**, *150*, 56. (c) Tolia, A. A.; Williams, C. T.; Takoudis, C. G.; Weaver, M. J. *J. Phys. Chem.* **1995**, *99*, 4599. (d) Williams, C. T.; Tolia, A. A.; Chan, H. Y. H.; Takoudis, C. G.; Weaver, M. J. *J. Catal.* **1996**, *163*, 63. (e) Chan, H. Y. H.; Takoudis, C. G.; Weaver, M. J. *J. Catal.* **1997**, *172*, 336. (f) Williams C. T.; Takoudis, C. G.; Weaver, M. J. *J. Phys. Chem. B* **1998**, *102*, 406. (g) Chan, H. Y. H.; Williams, C. T.; Weaver, M. J.; Takoudis, C. G. *J. Catal.* **1998**, *174*, 191. (h) Williams, C. T.; Chen, E. K.-Y.; Takoudis, C. G.; Weaver, M. J. *J. Phys. Chem. B* **1998**, *102*, 4785.

(6) Pettinger, B. In *Adsorption of Molecules at Metal Electrodes*; Lipkowski, J., Ross, P. N., Eds.; VCH Publishers: New York, 1992; Chapter 6.

(7) (a) Zou, S.; Weaver, M. J. *Anal. Chem.* **1998**, *70*, 2387. (b) Zou, S.; Gomez, R.; Weaver, M. J. *Langmuir* **1997**, *13*, 6713.

(8) (a) Zou, S.; Williams, C. T.; Chen, E. K.-Y.; Weaver, M. J. *J. Am. Chem. Soc.* **1998**, *120*, 3811. (b) Zou, S.; Williams, C. T.; Chen, E. K.-Y.; Weaver, M. J. *J. Phys. Chem. B* **1998**, *102*, 9039, 9743.

(9) Gao, X.; Zhang, Y.; Weaver, M. J. *Langmuir* **1992**, *8*, 668.

(10) Wilke, T.; Gao, X.; Takoudis, C. G.; Weaver, M. J. *J. Catal.* **1991**, *130*, 62.

(11) Gao, P.; Gosztola, D.; Leung, L.-W. H.; Weaver, M. J. *J. Electroanal. Chem.* **1986**, *209*, 377.

(12) Parker, D. H.; Bartram, M. E.; Koel, B. E. *Surf. Sci.* **1989**, *217*, 489.

(13) Imbihl, R.; Demuth, J. E. *Surf. Sci.* **1986**, *173*, 395.

(14) (a) Marinov, T. S.; Kostov, K. L. *Surf. Sci.* **1987**, *185*, 203. (b) Davis, J. E.; Nolan, P. D.; Karseboom, S. G.; Mullins, C. B. *J. Chem. Phys.* **1997**, *107*, 943.

(15) (a) Root, T. W.; Fisher, G. B.; Schmidt, L. D. *J. Chem. Phys.* **1986**, *85*, 4687. (b) Wagner F. T.; Moylan, T. E. *Surf. Sci.* **1987**, *191*, 121.

(16) Dubois, L. H. *J. Chem. Phys.* **1982**, *77*, 5228.

(17) (a) Thomas, G. E.; Weinberg, W. H. *J. Chem. Phys.* **1979**, *70*, 954. (b) Mitchell, W. J.; Weinberg, W. H. *J. Chem. Phys.* **1996**, *104*, 9127. (c) He, P.; Jacobi, K. *Phys. Rev. B* **1997**, *55*, 4751.

(18) Graham, G. W.; Weber, W. H.; McBride, J. R.; Peters, C. R. *J. Raman Spectrosc.* **1991**, *22*, 1.

(19) (a) Weber, W. H.; Baird, R. J.; Graham, G. W. *J. Raman Spectrosc.* **1988**, *19*, 239. (b) McBride, J. R.; Hass, K. C.; Weber, W. H. *Phys. Rev. B* **1991**, *44*, 5016.

(20) (a) Liao, P. C.; Chen, C. S.; Ho, W. S.; Huang, Y. S.; Tiong, K. K. *Thin Solid Films* **1997**, *301*, 7. (b) Liao, P. C.; Ho, W. S.; Huang, Y. S.; Tiong, K. K. *J. Mater. Res.* **1998**, *13*, 1318. (c) Huang, Y. S.; Lin, S. S.; Huang, C. R.; Lee, M. C.; Dann, T. E.; Chien, F. Z. *Solid State Commun.* **1989**, *70*, 517.

(21) Mar, S. Y.; Chen, C. S.; Huang, Y. S.; Tiong, K. K. *Appl. Surf. Sci.* **1995**, *90*, 479.

(22) (a) Griffith, W. P. *J. Chem. Soc. A* **1968**, 1663. (b) Levin, I. W. *Inorg. Chem.* **1969**, *8*, 1018.

(23) Benziger, J. B.; Pascal, F. A.; Bernasek, S. L.; Soriaga, M. P.; Hubbard, A. T. *J. Electroanal. Chem.* **1986**, *198*, 65.

(24) Burke, L. D.; Buckley, D. T. *J. Electroanal. Chem.* **1994**, *366*, 239.

(25) Chausse, V.; Regull, P.; Victori, L. *J. Electroanal. Chem.* **1987**, *238*, 115.

(26) (a) Burke, L. D.; Lyons, M. E. G. In *Modern Aspects of Electrochemistry*; White, R. E., Bockris, J. O'M., Conway, B. E., Eds.; Plenum: New York, 1986; Vol. 18; Chapter 4. (b) O'Sullivan, E. J. M.; Calvo, E. J. In *Comprehensive Chemical Kinetics*; Compton, R. G., Ed.; Elsevier: Amsterdan, 1987; Vol. 27, Chapter 3.

(27) (a) Mozota, J.; Conway, B. E. *Electrochim. Acta* **1983**, *28*, 1. (b) Conway, B. E.; Mozota, J. *Electrochim. Acta* **1983**, *28*, 9.

(28) Kötz, R.; Stucki, S.; Scherson, D.; Kolb, D. M. *J. Electroanal. Chem.* **1984**, *172*, 211.

(29) van de Geest, M. E.; Dangerfield, N. J.; Harrington, D. A. *J. Electroanal. Chem.* **1997**, *420*, 89.

(30) (a) Mallika, C.; Sreedharan, O. M.; Gnanamoorthy, J. B. *J. Less Common Met.* **1983**, *95*, 213. (b) Bell, W. E.; Inyard, R. E.; Tagami, M. *J. Phys. Chem.* **1966**, *70*, 3735.

(31) (a) Mallika, C.; Sreedharan, O. M.; Chandrasekharaiah, M. S. *J. Less Common Met.* **1985**, *107*, 203. (b) Cordfunke, E. H. P. *Thermochim. Acta* **1981**, *50*, 177.

(32) Chatteji, D.; Vest, R. W. *J. Am. Ceram. Soc.* **1971**, *54*, 73.

(33) Goldberg, R. N.; Hepler, L. G. *Chem. Rev.* **1968**, *68*, 229.

(34) Mrozek, M.; Weaver, M. J. *J. Am. Chem. Soc.*, in press.

(35) Chan, H. Y. H.; Takoudis, C. G.; Weaver, M. J. *Electrochem. Solid State Lett.* **1999**, *2*, 189.

(36) Weaver, M. J.; Williams, C. T.; Zou, S.; Chan, H. Y. H.; Takoudis, C. G. *Catal. Lett.* **1998**, *52*, 181.

(37) (a) Peuckert, M. *J. Phys. Chem.* **1985**, *89*, 2481. (b) The "dissociation pressure" is defined as the pressure of oxygen in equilibrium with the bulk-phase oxide at a given temperature.

(38) Peuckert, M.; Bonzel, H. P. *Surf. Sci.* **1984**, *145*, 239.

(39) Berry, R. J. *Surf. Sci.* **1978**, *76*, 415.

(40) Kim, K. S.; Gossmann, A. F.; Winograd, N. *Anal. Chem.* **1974**, *46*, 197.

(41) Bondzie, V. A.; Kleban, P.; Dwyer, D. J. *Surf. Sci.* **1996**, *347*, 319.

(42) Voogt, E. H.; Mens, A. J. M.; Gijzeman, O. L. J.; Geus, J. W. *Surf. Sci.* **1997**, *373*, 210.

(43) Marinova, Ts. S.; Kostov, K. L. *Surf. Sci.* **1987**, *185*, 203.

(44) Kellogg, G. L. *Surf. Sci.* **1986**, *171*, 359.

(45) Logon, A. D.; Datye, A. K.; Houston, J. E. *Surf. Sci.* **1991**, *245*, 280.

(46) Nolan, P. D.; Wheeler, M. C.; Davis, J. E.; Mullins, C. B. *Acc. Chem. Res.* **1998**, *31*, 798.

(47) One anticipates that oxygen is bound in 4-fold hollow sites on Rh(100)[16] and 3-fold sites on Rh(111).[13] The lower ν_{M-O} value for the former system is consistent with such differing binding geometries.[48]

(48) Anderrson, S. *Chem. Phys. Lett.* **1978**, *55*, 185.

(49) Ramsier, R. D.; Gao, Q.; Waltenberg, N. H.; Lee, K.-W.; Nooij, O. W.; Lefferts, L.; Yates, J., Jr. T. *Surf. Sci.* **1994**, *320*, 209.

(50) (a) Rotermund, H. H.; Lauterbach, J.; Haas, G. E. *Appl. Phys. A* **1993**, *57*, 507. (b) Lauterbach, J.; Asakura, K.; Rotermund, H. H. *Surf. Sci.* **1994**, *313*, 52. (c) von Oertzen, A.; Mikhailov, A.; Rotermund, H. H.; Ertl, G. *Surf. Sci.* **1996**, *350*, 259.

(51) He, J.-W.; Memmert, U.; Norton, P. R. *J. Chem. Phys.* **1989**, *90*, 5088.
(52) Ladas, S.; Kennou, S.; Hartmann, N.; Imbihl, R. *Surf. Sci.* **1997**, *382*, 49.
(53) (a) Parker, D. H.; Koel, B. E. *J. Vac. Sci. Technol. A* **1990**, *8*, 2585. (b) Saliba, N. A.; Tsai, Y.-L.; Panja, C.; Koel, B. E. *Surf. Sci.* **1999**, *419*, 79.
(54) (a) Parker, D. H.; Bartram, M. E.; Koel, B. E. *Surf. Sci.* **1989**, *217*, 489. (b) Banse, B. A.; Koel, B. E. *Surf. Sci.* **1990**, *232*, 275.
(55) Peterlinz, K. A.; Sibener, S. J. *J. Phys. Chem.* **1995**, *99*, 2817.
(56) (a) Mitchell, W. J.; Weinberg, W. H. *J. Chem. Phys.* **1996**, *104*, 9127. (b) Hrbek, J.; van Campen, D. J.; Malik, I. J. *J. Vac. Sci. Technol. A* **1995**, *13*, 1409. (c) Böttcher, A.; Niehus, H. *J. Chem. Phys.* **1999**, *110*, 3186.
(57) Gland, J. L. *Surf. Sci.* **1980**, *93*, 487.
(58) Neuhas, D.; Joo, F.; Feuerbacher, B. *Phys. Rev. Lett.* **1987**, *58*, 694.
(59) For example: (a) Young, L. *Anodic Oxide Films*; Academic Press: New York, 1961. (b) Fromhold, A. T., Jr. *Theory of Metal Oxidation*; North-Holland Publishers: Amsterdam, 1976.
(60) Weaver, M. J. *J. Electroanal. Chem.* **1974**, *51*, 231.
(61) (a) Trasatti, S. *Electrochim. Acta* **1991**, *36*, 1659. (b) Trasatti, S. *Surf. Sci.* **1995**, *335*, 1 and previous references therein.
(62) For an erudite review, see: Wagner, F. T. In *Structure of Electrified Interfaces*; Lipkowski, J., Ross, P. N., Eds.; VCH Publishers: New York, 1993; Chapter 9.
(63) Villegas, I.; Gomez, R.; Weaver, M. J. *J. Phys. Chem.* **1995**, *99*, 14832.
(64) (a) Weaver, M. J.; Zou, S.; Tang, C. *J. Chem. Phys.* **1999**, *111*, 368. (b) Weaver, M. J. *Surf. Sci.* **1999**, *423*, 215.
(65) Rotermund, H. H.; Jakubith, S.; Kubala, S.; von Oertzen, A.; Ertl, G. *J. Electron Spectrosc. Relat. Phenom.* **1990**, *52*, 811.
(66) Chakraborty, B.; Holloway, S.; Norskov, J. K. *Surf. Sci.* **1985**, *152/153*, 660.
(67) (a) You, H.; Zurawski, D. J.; Nagy, Z.; Yonco, R. M. *J. Chem. Phys.* **1994**, *100*, 4699. (b) Tidswell, I. M.; Markovic, N. M.; Ross, P. M. *J. Electroanal. Chem.* **1994**, *376*, 119.
(68) Schneeweiss, M. A.; Kolb, D. M.; Liu, D.; Mandler, D. *Can. J. Chem.* **1997**, *75*, 1703 and references therein.
(69) Colum, F. In *Standard Potentials in Aqueous Solution*; Bard, A. J., Parsons, R., Jordan, J., Eds.; Marcel Dekker: New York, 1985; pp 343, 353, 383.
(70) Weaver, M. J. *Int. J. Mass Spectrom. Ion Processes* **1999**, *182/183*, 403.
(71) Weaver, M. J. *Top. Catal.* **1999**, *8*, 65.